Microbiological Research 301 (2025) 128310

Contents lists available at ScienceDirect

Microbiological Research

journal homepage: www.elsevier.com/locate/micres

Pirin, a redox-sensitive modulator of beta-oxidation, generates hydroxyl radicals and interacts with CatR, the transcriptional repressor of the major vegetative catalase gene in *Streptomyces*

Matteo Calcagnile [a,1], Fabrizio Damiano [a,1], Adelfia Talà [b], Pietro Alifano [a,*]

[a] Department of Experimental Medicine (DiMes), University of Salento, Lecce 73100, Italy
[b] Department of Biological and Environmental Sciences and Technologies (DiSTeBA), University of Salento, Lecce 73100, Italy

ARTICLE INFO

Keywords:
Pirin-like proteins
Aerobic energy metabolism
Beta-oxidation
Antioxidant systems
Catalase

ABSTRACT

Pirins are iron-containing proteins conserved throughout evolution, which have been implicated in diverse cellular processes, mostly associated with stress. In prokaryotes, Pirins are present in many taxonomic groups and can be present in multiple copies, and only a few of these proteins have been studied. In *Streptomyces ambofaciens* a Pirin-like protein, PirA, is a redox-sensitive negative modulator of AcdB, a very long-chain acyl-CoA dehydrogenase (vLCAD), which catalyzes the first committed step of the beta-oxidation pathway. In this study, we first classified the Pirins in different prokaryotic and non-prokaryotic taxa, and we found strong connections between the occurrence of Pirins and aerobic energy metabolism. We then studied whether the presence of Pirins is connected to the regulation of antioxidant systems, after observing that a *pirA*-defective mutant of *S. ambofaciens* accumulated large amounts of H_2O_2 during the vegetative growth. *In vitro* experiments suggested that the accumulation of H_2O_2 in the *pirA* mutant could be partially due to an increased vLCAD activity of AcdB, which releases H_2O_2 as a byproduct of the reaction. However, the reduction in catalase and alkylhydroperoxidase expression levels in the *pirA* mutant, despite the increased amount of intracellular H_2O_2, also indicated a dysregulation of these antioxidant systems. Indeed, the gene *catA* encoding the major vegetative catalase and the adjacent regulatory gene *catR* were down-regulated in the *pirA* mutant. In Gram-positive bacteria, CatR/PerR family regulators repress transcription of genes coding for the major vegetative catalase. These repressors are irreversible inactivated by hydroxyl radicals and detach from the DNA, which leads to de-repression of catalase expression. We found that PirA generates hydroxyl radicals after reacting with H_2O_2, and binds CatR *in vitro*, suggesting that by generating hydroxyl radicals in response to H_2O_2 exposure, PirA could promote CatR inactivation allowing *catA* transcription.

1. Introduction

Pirins are iron-containing proteins belonging to the cupin superfamily, which are found in all the kingdoms of life and have been implicated in diverse cellular processes, mostly associated with stress. Human Pirin (hPirin) was initially described as an NF-I/CTF interactor (Wendler et al., 1997), and it was later discovered its ability to form complexes with Bcl-3 and dimer of NF-κB on NF-κB binding sites to promote the transcription of anti-apoptotic genes (Dechend et al., 1999). These findings suggest an involvement of hPirin in transcription regulation and/or in other nuclear processes, although this function has recently been questioned (Gomez et al., 2023; Meschkewitz et al., 2023). Also in tomato, Pirin was involved in programmed cell death (Orzaez et al., 2001), while in *Arabidopsis thaliana* Pirin (AtPirin1) was implicated in regulation of seed germination (Lapik and Kaufman, 2003).

Studies on Pirin have also been conducted on bacteria. In cyanobacteria, a Pirin-encoding gene was shown to be strongly up-regulated under stress conditions such as severe salt stress (Hihara et al., 2004), while in the nitrifying *Nitrosomonas europaea* a Pirin-encoding ortholog was found to be highly induced during phenol exposure (Lauchnor et al., 2011). In *Serratia marcescens* Soo and colleagues (Soo et al., 2007) demonstrated that a gene coding for Pirin regulates the catabolism of pyruvate by interacting with the E1 subunit of pyruvate dehydrogenase. Two few years before, Adams and Jia (2005) determined the crystal

* Corresponding author.
E-mail address: pietro.alifano@unisalento.it (P. Alifano).
[1] These authors contributed equally

https://doi.org/10.1016/j.micres.2025.128310
Received 9 April 2025; Received in revised form 24 July 2025; Accepted 12 August 2025
Available online 13 August 2025

structure of the Pirin-encoding ortholog YhhW from *Escherichia coli*, and provided evidence that both hPirin and YhhW may act as 2,3-dioxygenases using the antioxidant quercetin as a substrate.

In actinomycetes a Pirin-encoding gene, *pirA*, plays an important role at the intersection of cellular metabolism and oxidative stress (Talà et al., 2018). In *Streptomyces ambofaciens pirA* contains an attachment site for the bacteriophage ΦC31, and the insertional inactivation of *pirA* by ΦC31 Att/Int system-based vectors produced marked effects on central carbon and energy metabolism, high sensitivity to H_2O_2, repression of polyketide antibiotic production, and substantial accumulation of total lipid esters in triacylglycerol (TAG) stores. Most of these effects could be traced to the inability of the *pirA*-defective strain to modulate the beta-oxidation pathway leading to metabolic unbalance. Indeed, biochemical evidence was provided that PirA interacts with very long-chain acyl-CoA dehydrogenase (vLCAD) AcdB, which catalyzes the first committed step of the beta-oxidation pathway, and is a redox-sensitive negative modulator of its activity (Talà et al., 2018).

In the present study we try to bring some of the different results obtained with the different organisms into a coherent model. To this purpose, we first attempted to classify the Pirin-like proteins in different bacterial and non-bacterial taxa, and found strongly connections between the presence of Pirin-like proteins and aerobic energy metabolism. We then studied whether the presence of Pirin-like proteins is connected to the regulation of antioxidant systems, investigating, both with *in vivo* and *in vitro* experiments, some aspects of the function of PirA of *S. ambofaciens*, starting from the evidence that a *pirA*-defective mutant accumulates greater amounts of H_2O_2 than the wild type parental strain. The study of the mechanisms underlying this accumulation of H_2O_2 has made it possible to discover new functions of PirA extendable to other Pirin-like proteins.

2. Materials and methods

2.1. Strains, media, and growth condition

S. ambofaciens ATCC 23877 (wild type) was obtained from the American Type Culture Collection (ATCC), while derivative strains *S. ambofaciens pirA*::pTYM-18 and *S. ambofaciens pirA*::pTYM-pirA have been described previously (Talà et al., 2018). The composition (per liter) of the media used in this study for *S. ambofaciens* growth and manipulation is reported here. *S. ambofaciens* was initially grown using the solid medium Mannitol Starch Agar (MSA, per liter: 20 g mannitol, 20 g starch, and 20 g agar). Kanamycin was added to the medium when required to a final concentration of 25 mg/L. Yeast Starch medium (per liter 10 g starch and 2 g yeast extract) was used to measure the H_2O_2 production of *wild-type* (WT) and recombinant strains. Growth experiments with palm oil were performed in the previously used minimal medium (MBM) (Calcagnile et al., 2018; Lounès et al., 1996). The minimal medium had the following composition per liter: 20 g NaCl, 5 g $CaCO_3$, 4 g glucose per liter, 2 g KH_2PO_4, 1 g $MgSO_4$, 15 mg $ZnSO_4$, and 0.3 mg $CoCl_2$, and 20 mM valine. 1 mL of a 1:10 palm oil - dimethyl sulfoxide (DMSO) solution was added to the minimal medium. 1 mL of DMSO was used as a control. Growth experiments of *S. ambofaciens* were performed at 28°C with shaking (200 rpm).

Plasmid manipulation and cloning were performed using *Escherichia coli* DH5α. Recombinant proteins were produced using *Escherichia coli BL21*(DE3) using LB broth or agar and incubating the cultures at 37°C and 250 rpm. When required, 100 mg/L of ampicillin was added to the medium.

The media were sterilized by autoclaving (121°C for 20 min). The solutions containing heat-sensitive compounds (glucose and valine), antibiotics, and the oil-DMSO solutions were sterilized by filtration (0.2 μm) and added in the media after autoclaving.

Growth in YS was monitored by dry weight measurement. 10 mL of bacterial suspension was sampled and centrifuged (4000 rpm, 20 min, 4°C). The pellet was dried for 24 h at 37°C before weighing. In contrast, the minimal medium contained a high amount of $CaCO_3$ which was insoluble and compromised the use of dry weight as a parameter to measure growth. Therefore, the BacTiter-Glo™ Microbial Viability Assay Kit (G8230, Promega) was used according to the supplier's instructions to measure growth in the minimal medium.

To assess statistically significant differences, a two-sample t-test with Welch's correction was used for pairwise comparisons. Statistical analysis was conducted using the ttest_ind() function from the scipy.stats Python module, with the parameter equal_var=False to implement Welch's correction. Significance was evaluated using a threshold of $\alpha = 0.05$. Differences were considered statistically significant when $p < 0.05$; otherwise, the null hypothesis was not rejected.

One-way analysis of variance (ANOVA) was used to assess differences among multiple sample groups. When ANOVA indicated significant differences ($p < 0.05$), Tukey's honestly significant difference (HSD) post-hoc test was performed to determine pairwise differences between groups and identify statistically non-significant groupings ($p > 0.05$). All statistical analyses were conducted using Python (version 3.10) with the scipy.stats and statsmodels libraries.

2.2. Production and purification of recombinant proteins

Purified recombinant AcdB and PirA were obtained as reported in previous study (Talà et al., 2018), and dialyzed in 20 mM phosphate buffer pH 7.4 using Spectra/Por dialysis tubing (Spectrum). *S. ambofaciens catR* cDNA was obtained by PCR amplification using the primers CatR-F/CatF, and *S. ambofaciens* DNA as a template (*Nde*I and *Hin*dIII restriction sites for cloning are underlined):

CatF: 5′-AAGCTTCATATGAGTGACCTACTGGAACG-3′

CatR-R: 5′-GAATTCAAGCTTCGCGGCCGCGCAGTTCGGGC-3′

The amplicon was digested using *Nde*I (NEB, R0111S) and *Hin*dIII (NEB, R0104S) enzymes according to the supplier's instructions and ligated into pET21b-V5. The production of V5-tagged CatR into bacterial lysate was verified by Western blotting using the anti-V5 antibody.

2.3. Quercetinase activity and H_2O_2 assays

The quercetinase activity assay was performed as previously described (Guo et al., 2019; Adams and Jia, 2005), based on the decrease in the absorbance maximum for quercetin, which occurs around 370 nm at pH 7.5. Briefly, the reaction buffer consisted of 50 mM NaH_2PO_4 (pH 7.5), 150 mM NaCl, 50 μM quercetin, 5 % (v/v) DMSO, and 3 μM recombinant PirA protein. Reactions were conducted for 5 min at 25 °C. Change in the absorbance (370 nm) was monitored using a DU 800 Spectrophotometer reader (Beckman Coulter).

For H_2O_2 production by the recombinant purified AcdB protein, the assay mixture (1.5 mL) consisted of 50 mM potassium phosphate (pH 7.4), 500 ng horseradish peroxidase, 200 ng AcdB, and 200 ng-1μg PirA, along with 10 μM palmitoyl-CoA. After equilibration at 25 °C for 5 min, 500 nM DCF (H2DCFDA, Thermo Fisher) was added to initiate the reaction. Fluorescence reading was performed after a 30-second interval and continued for a total duration of 5 min. The excitation and emission wavelengths were 495 and 530 nm, respectively.

To evaluate the effect of PirA on H_2O_2 in the absence or in the presence of quercetin, assays were performed using the same scheme as previously described, with the addition of 500 μM H_2O_2, 100 μM quercetin, and 1 μg of PirA or human ATF6α, as reported in the figure.

H_2O_2 production by *S. ambofaciens* ATCC 23877 (wild type), *S. ambofaciens pirA*::pTYM-18 and *S. ambofaciens pirA*::pTYM-pirA grown in YS medium was performed as follows. 1 mg wet mycelium was washed twice with YS medium, and resuspended into 1.5 mL of YS medium. 500 nM DCF was added, and the fluorescence was monitored as previously described·H_2O_2 production by *S. ambofaciens* ATCC 23877 (wild type), *S. ambofaciens pirA*::pTYM-18 and *S. ambofaciens pirA*::pTYM-pirA grown in the minimal medium was determined as follows. The bacteria were grown on MSA agar for 72 h. Subsequently, a colony

was picked and inoculated into the minimal medium. After 72 h, 80 µL of bacterial suspension was picked and 1.6 µL of DMSO-oil solution or DMSO alone (control) was added. The obtained samples were treated using the ROS-Glo™ H_2O_2 Assay KIT (G8820, Promega) following the supplier's instructions. The bacterial suspensions were incubated for 24 h at 200 rpm and 28°C. After this time, the detection solution provided in the Kit (G8820, Promega) was added and the samples were incubated for 20 min at room temperature. The luminescence was measured using the Promega Glomax 20/20 luminometer.

Statistical analysis was performed using Welch's *t*-test as previously described.

2.4. ECL assay

Nitrocellulose membrane (BioTrace NT, Pall Life Science) was equilibrated with Transfer buffer (48 mM Tris-HCl, pH 9.2, 39 mM Glycine, 20 % methanol, 1.3 mM SDS). Then, recombinant PirA or hATF6α was loaded on the membrane by a slot blot manifold. After protein loading, the membrane was equilibrated with TBS-0.1 % Tween. Chemiluminescence developed by PirA was detected using the Pierce™ ECL Western Blotting Substrate (Thermo Fisher), and acquired through the ChemiDoc Imaging System (BioRad Laboratories). Statistical analysis was performed using Welch's *t*-test as previously described.

2.5. In vitro and in silico protein-protein interaction

The interaction between recombinant PirA and CatR proteins was assayed *in vitro* by co-elution experiment using the affinity chromatography, as described previously (Talà et al., 2018) with minimal modifications. 300 µg of clarified cell lysates from *E. coli* BL21(DE3) transformed with pET-CatR-V5 or pET-PirA-V5/His6 were mixed together and further processed as previously described (Talà et al., 2018). The protein complex CatR-V5:PirA-V5/His6 was then eluted with 50 µl of elution buffer (20 mM Tris–HCl pH 8.0, 500 mM NaCl, 500 mM imidazole and 10 % glycerol) for 1 h, at 4 °C. Eluted proteins were fractionated by sodium dodecyl sulfate polyacrylamide gel electrophoresis (SDS-PAGE) and electrophoretically transferred onto a nitrocellulose membrane (BioTrace NT, Pall Life Science), according to standard procedures. To detect V5-tagged proteins, the membrane was incubated with the antibody against V5 epitope. The negative control experiment was performed similarly, incubating equal amounts of clarified cell lysates from *E. coli* BL21(DE3) transformed with pET-CatR-V5 and pET-HsATF6α-His6, respectively. Any nonspecific complexes were then ruled out by co-eluting CatR-V5:HsATF6α-His6, as reported above. The input lysates and eluted proteins were analyzed by Western blot and sequentially probed with antibodies against the His and V5 epitopes.

The effect of the redox condition on the interaction between CatR and PirA was also evaluated. 300 ng of purified recombinant PirA-His or human ATF6α-His was loaded onto nitrocellulose membrane using a slot blot manifold. After a brief wash with TBS-0.1 % Tween, the membranes were incubated in 1 mL of 100 mM phosphate buffer (pH 7.4) with either 100 µM K3[Fe(CN)6] (Fe^{3+}) or K4[Fe(CN)6] · 3 H_2O (Fe^{2+}) for 1 h. Subsequently, the membrane was incubated with 300 µg of clarified cell lysates from *E. coli* BL21(DE3) transformed with pET-CatR-V5 for 1 h. The control experiment was conducted similarly, incubating 300 µg of clarified cell lysates from *E. coli* BL21(DE3) transformed with empty pET vector. After three washes with TBS-0.1 % Tween, the membranes were immunodecorated with anti-V5 antibody, and the chemiluminescence acquired with the ChemiDoc Imaging System (BioRad Laboratories).

In silico prediction of the complex was carried out using AlphaFold 3 (Abramson et al., 2024). The protein sequences of CatR (WP_003973766.1) and PirA (WP_053134172.1), along with the DNA sequence TTAGACAATGTCCAT, were submitted to the AlphaFold 3 server. CatR from *S. ambofaciens* was hypothesized to form a dimer, consistent with crystallographic models of Fur family transcriptional regulators (Lucarelli et al., 2007; Sarvan et al., 2018; Traoré et al., 2006).

2.6. Phylogenetic analysis, protein visualization and prediction of CatR-binding sites

A preliminary analysis of proteins annotated as Pirin-like was performed using the PFAM database (InterPro) (Paysan-Lafosse et al., 2023). Pirin-like proteins are bicupines and, therefore, have two domains. The first domain (N-terminal domain) is conserved in all pirins (Pirin_N_dom, PF02678). The second domain is variable and can be either a C-terminal domain common in Pirin proteins (Pirin_C_dom, PF05726) or a C-terminal domain present in quercetinases (Pirin_C_2, PF17954). All these domain architectures were used as queries for Pirin-like protein research. The search on InterPro was performed considering Pirin-like proteins with known function and present in humans, *S. ambofaciens*, *Serratia marcescens* and *Escherichia coli*. The protein sequences of Pirin-like proteins from these organisms were analyzed and used to identify similar proteins in other bacteria belonging to the phyla Pseudomonadota and Actinomycetota. Furthermore, Pirin-like sequences were identified in eukaryotic organisms belonging to the kingdoms Fungi, Plantae, and Animalia. The identified sequences were submitted to ClustalO (Sievers and Higgins, 2021) to obtain a phylogenetic tree. Subsequently, the tree was analyzed and manipulated using iTOL (Letunic and Bork, 2021). The same bioinformatic tools were used to perform phylogenetic analysis of catalase-encoding genes in *S. ambofaciens* and *S. coelicolor*. ClustalO (Sievers and Higgins, 2021) was also used to analyze sequence conservation in the CarR/PerR multiple alignment of deduced amino acid sequences.

Promoters containing putative CatR binding sites were identified in the genome of *S. ambofaciens* 23877 using the MEME suite (Bailey et al., 2015). Specifically, putative promoter sequences were extracted using BEDtools (Quinlan, 2014), considering the 200 bases upstream of the start of each gene. Subsequently, the conserved sequences of motifs previously described in the literature were obtained from *S. coelicolor* A3 (2) (Kim et al., 2021). Specifically, the CatR binding sequences identified in *catR*, *catA*, *vtlA*, and SCO4983 were used (Kim et al., 2021). The other motifs were identified in the upstream sequences of the same *S. ambofaciens* genes. The sequences were used to generate a matrix with the MEME tool, which was then submitted to FIMO (Grant et al., 2011) along with the promoter sequences extracted from the *S. ambofaciens* genome.

Crystallographic models of the *E. coli* YhhW (6UTS) (Guo et al., 2019), *Streptomyces* sp. FLA QueD (5FLI) (Jeoung et al., 2016), and hPIR protein (4EWA) (Liu et al., 2013) were identified in RCSB PDB (Berman et al., 2000). The model of the PirA protein form *S. ambofaciens* was derived from I-Tasser as previously described (Yang and Zhang, 2015). Whole protein structure analysis, metal cofactor binding site analysis, and result visualization were performed in Chimera UCSF (Pettersen et al., 2004).

2.7. Co-occurrence analysis and genome neighborhood analysis

String (Szklarczyk et al., 2023) was used to analyze genes that co-occur with the gene encoding Pirin-like proteins. The hPIR from *Homo sapiens* sequence (NP_001018119.1), the dhPIR protein sequence from *Debaryomyces hansenii* (XP_460132.1; DEHA2E19085p), and the PirA protein sequence from *S. ambofaciens* (ANB07461.1) were used as input. The results were analyzed using the co-occurrence function of String.

Using the EFI-EST tool (Oberg et al., 2023), the PirA protein sequence was used to calculate the synteny of genes close to the *pirA* in bacterial genomes. The PirA protein sequence was used as input, selecting "BLAST Sequence" as an option. The network obtained from this tool was used as input for the analysis of the EFI-GNT tool (Oberg et al., 2023). The genetic maps and networks obtained allowed us to

analyze the co-occurrence and genomic proximity of genes close to the *pirA* gene. The networks were analyzed using Cytoscape (Shannon et al., 2003).

3. Results

3.1. Pirin-like proteins in prokaryotic and non-prokaryotic taxa: the connection with aerobic energy metabolism

The genome of streptomycetes contains different paralogs encoding Pirin family proteins. We started this study with a phylogenetic analysis to classify these proteins. Using the Uniprot database as a source of Pirin family proteins from different prokaryotic and eukaryotic taxa, the Pirin-like protein family members could be classified into three major clusters and five sub-clusters (Fig. 1). The first two clusters include bacterial quercetinase D (QueD)-like proteins and bacterial YhaK-like proteins, including *E. coli* YhhW (WP 000639811.1) with proven quercetinase activity (Adams and Jia, 2005) and YahK (WP 000633576.1) devoid of this activity (Gurmu et al., 2009). The third cluster includes three sub-clusters: two sub-clusters of bacterial Pirin-like proteins (named bacterial Pirin-like proteins A and B) and one sub-cluster of eukaryotic Pirin-like proteins. The sub-cluster of bacterial Pirin-like proteins A includes the PirA protein from *S. ambofaciens* (WP 053134172.1) (Talà et al., 2018), while the prototype of bacterial Pirin-like proteins B is a protein from *S. marcescens* (WP 118892684.1) that interacts with the E1 subunit of pyruvate dehydrogenase (Soo et al., 2007). The sub-cluster of eukaryotic Pirin-like proteins include Pirin-like proteins of animals, plants and fungi, forming three distinct groups.

It may be noted that YhaK-like proteins and Pirin-like proteins share the Pirin N-terminal cupin domain (PF02678) but harbor different C-terminal domains. The YhaK-like proteins harbor the quercetinase C-terminal cupin domain (PF17954), while Pirin-like proteins are characterized by the Pirin C-terminal cupin domain (PF05726) (Fig. 1). This preliminary analysis demonstrates that bacterial Pirin-like proteins belong to two distinct sub-clusters (bacterial Pirin-like proteins A and B), in addition to the cluster of YhaK-like proteins.

We used STRING for the occurrence/co-occurrence analysis of Pirin family proteins in different taxa (Fig. S1). As input sequences, we used the human Pirin-like protein (hPirin) (NP 001018119.1) (Fig. S1A), *S. ambofaciens* PirA (Fig. S1B and Fig. S2), or *Debaryomyces hansenii* pirin-like protein (XP 460132.1; DEHA2E19085p) (Fig. S3). The results show that hPirin/PirA orthologs are present in most of prokaryotic and non-prokaryotic taxa with aerobic or facultative aerobic/anaerobic metabolism, with some exceptions, and absent in anaerobic organisms. Indeed, in protozoa, hPirin (Fig. S1A) and *S. ambofaciens* PirA (Fig. S2)

Fig. 1. Cladogram of Pirin-like proteins from different prokaryotic and eukaryotic taxa. The cladogram illustrates the taxonomic position of *S. ambofaciens* PirA (WP_053134172.1) with respect to other family members. The blue box represents QueD-like proteins, the yellow box represents eukaryotic PirA-like proteins, the pink boxes represent bacterial PirA-like proteins (PirA-like A and PirA-like B), and the green box represents Yhak-like proteins. The colored text highlights proteins with known functions: blue represents Human Pirin (hPirin), pink indicates Yhak-like proteins from *E. coli*, and green denotes proteins described as metabolism regulators (PirA from *S. ambofaciens* and PirA-like from *S. marcescens*). Pirin-like with unassigned functions are reported in black.

orthologs are absent in anaerobic protozoan parasites such as *Giardia* (phylum Metamonada), *Entamoeba* (phylum Sarcomastigophora/ Amoebozoa) and *Cryptosporidium* (phylum Apicomplexa). However, hPirin and *S. ambofaciens* PirA orthologs are also absent in trypanosomatids (Euglenozoa) of the genera *Trypanosoma* and *Leishmania*. The possible reason for the absence of hPirin/PirA in these aerobically metabolizing protozoa will be discussed below. All animals belonging to the phylum of Chordata harbors hPirin and *S. ambofaciens* PirA orthologs except those belonging to the class of Aves, as discussed below. hPirin and *S. ambofaciens* PirA orthologs are also absent in several strictly anaerobic Archaea (Thermococcales, Methanococcales, Archaeoglobales, Nitrosopumilales). In fungi, it may be noted the absence of genes encoding pirin-like proteins in Crabtree-positive yeasts *Saccharomyces cerevisiae* and *Schizosaccharomyces pombe*, as well as in taxa phylogenetically close to this latter including *Pneumocystis murina* and *Taphrina deformans* (Fig. S3).

3.2. Genes encoding pirin-like proteins in actinomycetes

In bacteria, the position of a gene in the genome relative to nearby genes can provide some clues about its function. In the genetic map of *S. ambofaciens* ATCC 23877, *pirA* is located in a rather conserved chromosomal region (Fig. 2A). Upstream of *pirA* it may be noted the presence of *sseB* (encoding a cyanide sulfurtransferase [TST], also named rhodanese), *acdB* (encoding a vLCAD), *apeB* (coding for an aspartyl aminopeptidase), a gene coding for a conserved protein with DUF6458 domain, and a gene coding for a lysine-oxoglutarate reductase (LOR)-related protein. Downstream of *pirA*, *perM* (coding for a permease), *spoEII* (coding for sporulation-related protein SpoEII) and *aspS* (encoding an aspartyl-tRNA synthetase) are located.

STRING analysis revealed the presence of *pirA* in most of actinobacterial genomes, except those of anaerobic actinomycetaceae (*Actinomyces*, *Mobilincus*, *Actinobaculum*, *Arcanobacterium*, *Varibaculum*), *Actinopolyspora* (fam. Actinopolysporaceae), and motile spore-bearing, iron-depositing Kineosporiaceae (Fig. 2B). This result is consistent with the absence of of *pirA* orthologs in most anaerobic bacterial taxa (Fig. S1B). STRING analysis also showed co-occurrence of *pirA* with *acdB* and with the other genes in the *S. ambofaciens pirA* chromosomal region (Fig. 2B). In the genome of all Streptomycetaceae (Streptomyces, Kitasaspora, Streptacidiphilus) and *Catenulispora* (fam. Catenulisporaceae) it may be also noted co-occurrence with *sseB* coding for rhodanese (Fig. 2B). Rhodanese is a widely distributed enzyme in both prokaryotes and eukaryotes, where it plays a relevant role in mitochondrial activity (Buonvino et al., 2022; Cipollone et al., 2007; Kruithof et al., 2020). This enzyme is involved in several processes including cyanide detoxification, sulfur and selenium metabolism, restoration of iron–sulfur clusters, redox system maintenance, and, in eukaryotes, mitochondrial import of 5S rRNA. Co-occurrence values were then calculated by EFI-EST (Fig. 2C) by using reference genomes of actinobacteria (Fig. 2D). The results showed highest values of co-occurrence with *pirA* (>80 %) for *sseB*, *acdB*, and *apeB*.

3.3. Streptomyces pirA inactivation leads to increased H_2O_2 levels

In *S. ambofaciens* ATCC 23877, insertional inactivation of *pirA* by the integrative plasmid pTYM-18 was shown to increase sensitivity of the

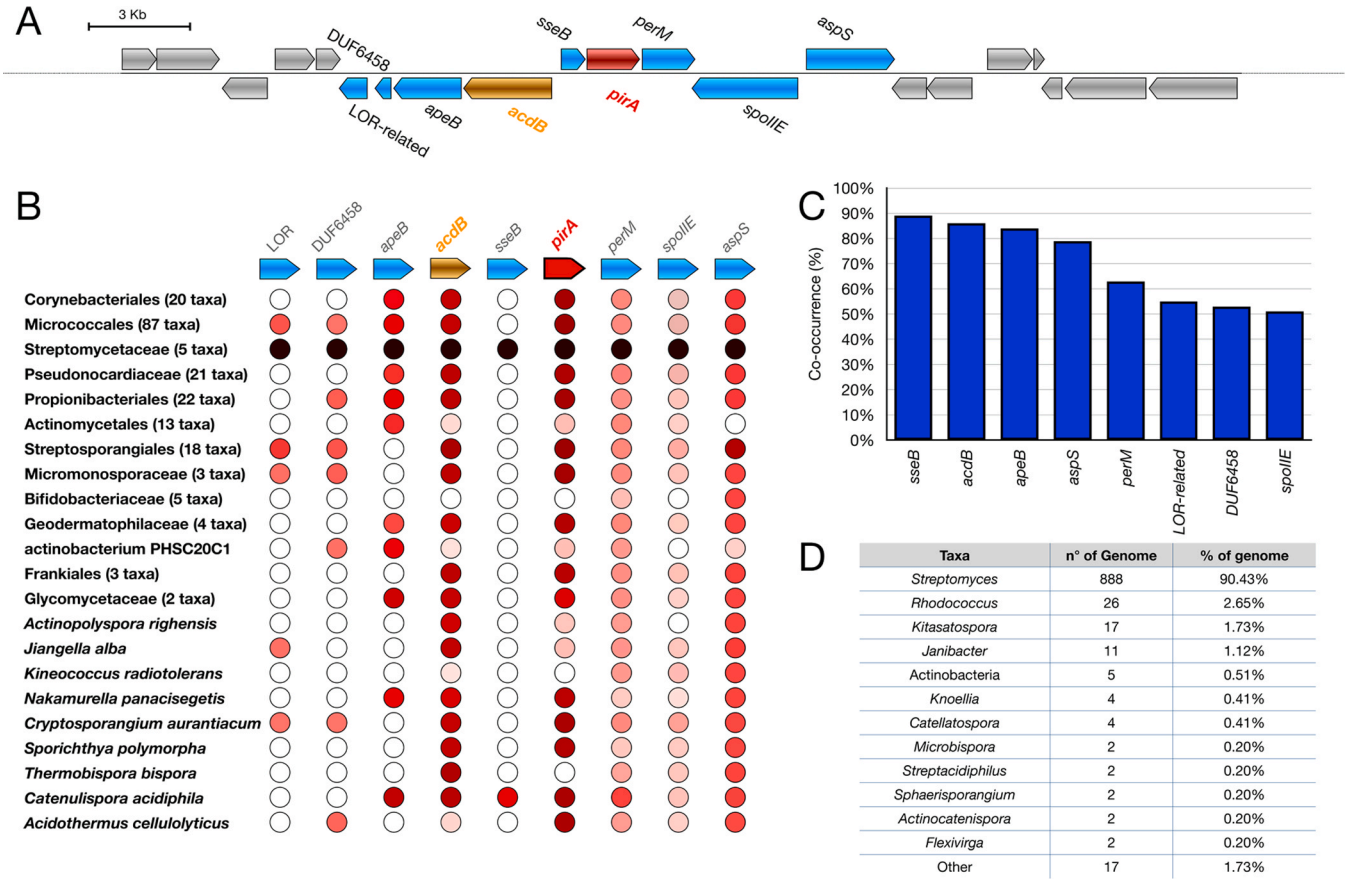

Taxa	n° of Genome	% of genome
Streptomyces	888	90.43%
Rhodococcus	26	2.65%
Kitasatospora	17	1.73%
Janibacter	11	1.12%
Actinobacteria	5	0.51%
Knoellia	4	0.41%
Catellatospora	4	0.41%
Microbispora	2	0.20%
Streptacidiphilus	2	0.20%
Sphaerisporangium	2	0.20%
Actinocatenispora	2	0.20%
Flexivirga	2	0.20%
Other	17	1.73%

Fig. 2. Co-occurrence and genomic proximity (synteny) analysis performed by EFI-EST, EFI-GNT, and STRING. A) Genetic map of the locus containing the *pirA* gene of *S. ambofaciens* showing the *pirA* gene (red), the *acdB* gene (yellow), genes co-occurring near the *pirA* locus (blue), and all other genes (grey). B) Co-occurrence analysis performed by STRING and PirA from *S. ambofaciens* as input, showing gene co-occurrence in taxa belonging to the phylum Actinomycetota. C) Co-occurrence and synteny analysis performed by EFI-EST and EFI-GNT, indicating the percentage (%) of genomes in which the reported genes are syntenic with *pirA*. D) Genomes identified by EFI-EST and EFI-GNT, on which synteny analysis was performed.

resulting strain *S. ambofaciens pirA*::pTYM-18 to H_2O_2 compared to the wild type strain (Talà et al., 2018). Here we hypothesized that the increased sensitivity of the *pirA*-defective strain to H_2O_2 could be due to an increased endogenous production of H_2O_2 which can saturate the cellular antioxidant capacity and/or to a decreased removal of H_2O_2 by catalase or alkylhydroperoxidase. In both cases, we expected an increase in intracellular H_2O_2 levels in the *pirA*-defective strain.

Therefore, we monitored the production of H_2O_2 during the growth of the wild type strain, the *pirA*-defective strain and a *pirA*-complemented strain in YS broth. We used a method based on the oxidation of the non-fluorescent probe 2′,7′-dichlorofluorescin (DCFH) to yield the highly fluorescent 2′,7′-dichlorofluorescein (DCF) (LeBel et al., 1992). In cells, H_2O_2 induces DCF formation in the presence of ferrous iron, while superoxide anion does not directly oxidize DCHF (LeBel et al., 1992), thus this simple method could be used to assay H_2O_2 in the mycelium.

S. ambofaciens growth was stopped at different time points (Fig. 3A), and the results of the DCFH assay showed that during the late exponential phase (48 h) and the early stationary phase (72 h), and to a much lesser extent also during the second stationary phase (96 h), the fluorescence was statistically significantly (p-value <0.05) increased in the *pirA*-defective strain compared to the wild-type strain and the *pirA*-complemented strain (Fig. 3B). In contrast, no significant differences were observed between strains in the early exponential phase (24 h). This result indicated that genetic inactivation of *pirA* resulted in increased intracellular H_2O_2 levels during late exponential and early stationary phases.

The wild-type, *pirA*- defective and *pirA*-complemented strains of *S. ambofaciens* were then grown in minimal medium supplemented with 1 mL of a 1:10 solution of palm oil in DMSO. Palm oil consists of a mixture of fatty acids, with palmitic acid being the main component, representing more than 40 % of the total fatty acids (Mancini et al., 2015). As previously shown, the vLCAD AcdB utilizes palmitoyl-CoA (Talà et al., 2018). The growth of the strains was monitored by luminescence-based ATP assay, as described in the Materials and Methods section, because the medium used was rich in $CaCO_3$, which is insoluble at the concentration used in the minimal medium, making measurements based on dry weight inaccurate. As a control, the three strains were grown in minimal medium supplemented with DMSO without palm oil.

The growth curves are shown in Fig. 3C. As observed, the three strains grown in the control medium exhibited similar growth patterns, and the Welch's *t*-test confirms that the values obtained were not statistically different (*p*-value > 0.05). When palm oil was added to the minimal medium, all three strains exhibited reduced growth compared

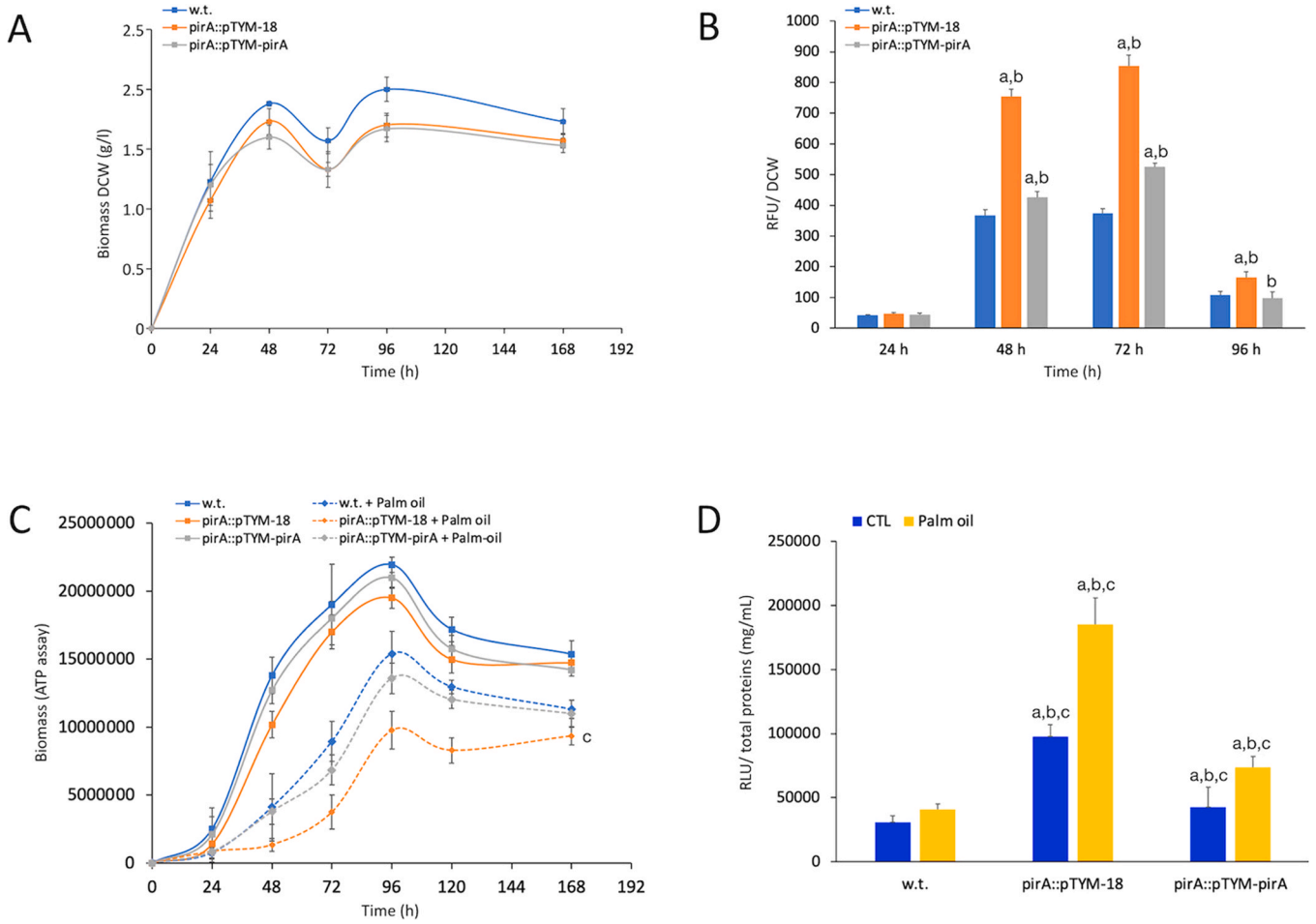

Fig. 3. *S. ambofaciens* ATCC 23877 growth curves and H_2O_2 production. A-B**)** Growth curves (A) and H_2O_2 production (B) of *S. ambofaciens* ATCC 23877, isogenic *pirA* mutant and *pirA*-complemented strain. The strains were grown in YS broth·H_2O_2 production was revealed by dichlorofluorescein (DCF) assay as described in the Materials and Methods section. C) Growth curves of *S. ambofaciens* ATCC 23877, isogenic *pirA* mutant, and *pirA*-complemented strain. The strains were grown in the minimal medium supplemented with 1 mL of DMSO or 1 mL of a 1:10 solution of palm oil in DMSO. D) H_2O_2 production of *S. ambofaciens* ATCC 23877, isogenic *pirA* mutant and *pirA*-complemented strain. The strains were grown in the minimal medium for 72 h, then 1.6 µL of DMSO-oil solution or DMSO alone (control) was added, and after 24 h the H_2O_2 production was revealed as described in the Materials and Methods section. Statistical significance was reported as follows: a = p-value < 0.05 of w.t. *vs* pirA::pTYM-18 or w.t. *vs* pirA::pTYM-pirA samples; b = p-value < 0.05 of pirA::pTYM-18 *vs* pirA::pTYM-pirA samples; c = p-value < 0.05 of palm-oil *vs* CTL samples.

to the controls, with the decrease being more pronounced in the *pirA*-defective strain. The *p*-value calculations indicated no significant difference in growth between the original strain and the complemented strain when comparing cultures grown with DMSO alone and those grown with the DMSO-palm oil solution (*p*-value > 0.05). In contrast, the *pirA*-defective strain showed a statistically significant difference (*p*-value $= 0.03853$).

An independent experiment was conducted to determine whether palm oil increased H_2O_2 production during growth in minimal medium. The three strains were first pre-cultured without DMSO or DMSO-oil. These cultures were then used as an inoculum for minimal medium containing either DMSO alone or DMSO-oil, as described in the Materials and Methods section. After 18 h of incubation, H_2O_2 production was measured. The values of H_2O_2 quantification were subsequently normalized to biomass. To achieve this, each culture was centrifuged, and the resulting pellet was resuspended in the same initial volume of culture medium. Total protein content was measured using the Bradford method, and biomass was expressed as total protein (mg) per milliliter of culture medium. Results indicated that supplementation with palm oil resulted in reduced growth of wild-type and *pirA*-complemented strains and, especially, the *pirA*-defective strain (Fig. 4 3 C). All three strains produced more H_2O_2 when grown with oil than without oil, indicating that beta-oxidation of palm oil fatty acids was a major source of H_2O_2 (Fig. 3D). However, only in the case of the *pirA*-complemented strain and the *pirA*-defective strain, the difference between the palm oil sample and the control samples was statistically significant (p-value <0.05). In addition, the increase in H_2O_2 production was moderate in the wild-type strain (32 %), it was higher in the *pirA*-complemented strain (73 %) and much higher (90 %) in the *pirA*-defective strain. Moreover, even in the absence of palm oil, H_2O_2 levels were higher in the *pirA*-defective strain than in the wild-type and *pirA*-complemented strains.

3.4. *Streptomyces AcdB (vLCAD) activity is a source of intracellular H_2O_2*

We hypothesized that the increased H_2O_2 production in the *pirA*-defective strain compared to the wild type and the *pirA*-complemented strain could be due, at least in part, to increased AcdB activity, a vLCAD, in the absence of PirA, based on previous study (Talà et al., 2018). In fact, in eukaryotes the vLCAD has residual oxidase activity which is known to release H_2O_2 (Doi et al., 2014; Kakimoto et al., 2015; Zhang et al., 2019).

Therefore, we analyzed whether *S. ambofaciens* AcdB produces H_2O_2 as a byproduct of reaction. In particular, production of H_2O_2 was measured during the reaction catalyzed by purified recombinant *S. ambofaciens* AcdB in the presence of palmitoyl-CoA as substrate. We used the method based on the oxidation of the non-fluorescent DCFH to yield the highly fluorescent DCF in the presence of H_2O_2 and horseradish peroxidase (HRP) as a catalyst. The results demonstrated that, indeed, AcdB produced H_2O_2 during the reaction and that the addition of PirA statistically significantly inhibited production of H_2O_2 in a dose-dependent manner (Fig. 4AB), which is consistent with the inhibition of AcdB activity by PirA (Talà et al., 2018).

As a control, we observed that *S. ambofaciens* PirA did not produce fluorescence in the presence of H_2O_2 and in the absence of HRP, while neither PirA nor a control protein (ATF6a) significantly affected fluorescence development in the presence of both of H_2O_2 and HRP (Fig. 4C). Furthermore, as expected, fluorescence development in the presence of both H_2O_2 and HRP was inhibited by quercetin, a plant flavonoid well known to scavenge H_2O_2 and reactive oxygen species (Papuc et al., 2017). However, it was noted that the inhibitory effect of quercetin was partially alleviated when PirA, but not ATF6a control protein, was added to the reaction, indicating an interaction between PirA and quercetin. Therefore, the quercetinase activity of PirA was assayed.

3.5. *Streptomyces PirA binds quercetin and has quercetinase activity*

Initial evidence demonstrated that both hPirin and *E. coli* YhhW are functionally similar to the cupin domain-containing enzyme quercetin 2,3-dioxygenases (QueD; EC 1.13.11.24) (Adams and Jia, 2005). These enzymes (also known as flavonol 2,4-dioxygenase or flavonol 2,3-dioxygenase) were characterized in different filamentous fungi such as *Aspergillus japonicus* (Steiner et al., 2002) and *Penicillium olsonii* (Tranchimand et al., 2008), and soil bacteria including *Bacillus subtilis* (Bowater et al., 2004), *Pseudomonas stutzeri* (Widiatningrum et al., 2015), and *Streptomyces* sp. FLA (Merkens et al., 2007), which are able to metabolize quercetin and other flavonols such as rutin that are abundantly found in vegetal tissues and exudates (Tranchimand et al., 2010). Indeed, both hPirin and *E. coli* YhhW may act as 2,3-dioxygenases using the antioxidant quercetin as a substrate. Quercetin 2,3-dioxygenase converts the quercetin to 2-protocatechuoylphloroglucinol carboxylic acid and carbon monoxide (Adams and Jia, 2005).

Thus, we first analyzed whether *Streptomyces* PirA is able to bind quercetin. *In silico* analysis (Fig. 4E) showed that the binding site of quercetin in the bacterial QueD, which is characterized by glutamic acid and three histidine residues, is conserved in *E. coli* YhhW, human hPirin, both possessing quercetinase activity, and *Streptomyces* PirA. *In silico* prediction were confirmed by *in vitro* experiments showing that the purified recombinant *S. ambofaciens* PirA has quercetinase activity *in vitro*, determined by measuring the decrease in the absorbance maximum for quercetin (384 nm at pH 8.0) (Adams and Jia, 2005), and the reaction rate was enhanced by addition of H_2O_2 (Fig. 4D).

3.6. *PirA reacts with H_2O_2 and generates hydroxyl radicals*

Streptomyces PirA was not able to convert DCFH into fluorescent DCF in the presence of H_2O_2 (Fig. 4C), a very indirect oxidative conversion that requires peroxidase activity, transition metals or heme enzymes (Kim et al., 2006). However, we noticed that in the presence of H_2O_2, PirA, but not ATF6a control protein, produced luminescence in the standard enhanced chemiluminescence (ECL) reaction with luminol (Fig. 5AB). The finding that PirA produced luminescence in the ECL reaction suggested that PirA may form hydroxyl radicals (OH•) in the presence of H_2O_2, through a Fenton-type reaction, as discussed below.

3.7. *Streptomyces pirA inactivation dysregulates catalase gene expression*

We initially thought that the increased H_2O_2 production in the *pirA*-deficient strain might be due to increased vLCAD activity of AcdB (releasing H_2O_2 as a byproduct of the reaction) in the absence of PirA. However, increased H_2O_2 production was expected to increase the expression of antioxidant enzymes, and instead proteomic analysis demonstrated down-regulation of catalase CatA (SAM23877_RS23675) (-1.9-fold), alkylhydroperoxidase (SAM23877_RS02130) (-1.5-fold), and superoxide dismutase SodF (SAM23877_RS12605) (-1.4-fold) in the *pirA*-deficient strain compared to the wild-type strain (Talà et al., 2018). This finding led us to hypothesize a dysregulation of the CatR regulon, the systems involved in the protection of *Streptomyces* spp. from reactive oxygen species (Kim et al., 2021), in the *pirA*-deficient strain. Therefore, the next step was to characterize the *S. ambofaciens* genes encoding antioxidant systems based on available genomic information.

3.8. *The antioxidant systems in S. ambofaciens*

The genome of *S. ambofaciens* ATCC 23877 contains 3 genes that codes for catalases (SAM23877_RS03710; SAM23877_RS23675; SAM23877_RS28230, respectively), a gene for a hydroperoxidase II (SAM23877_RS32650 [*katE/catB*]), and a gene for a catalase/peroxidase HPI (SAM23877_RS33045 [*katG*]). In the genome of the model actinomycete *Streptomyces coelicolor* A3(2), a similar enzymatic complement occurs, with 3 genes that code for catalases (FQ762_RS32085;

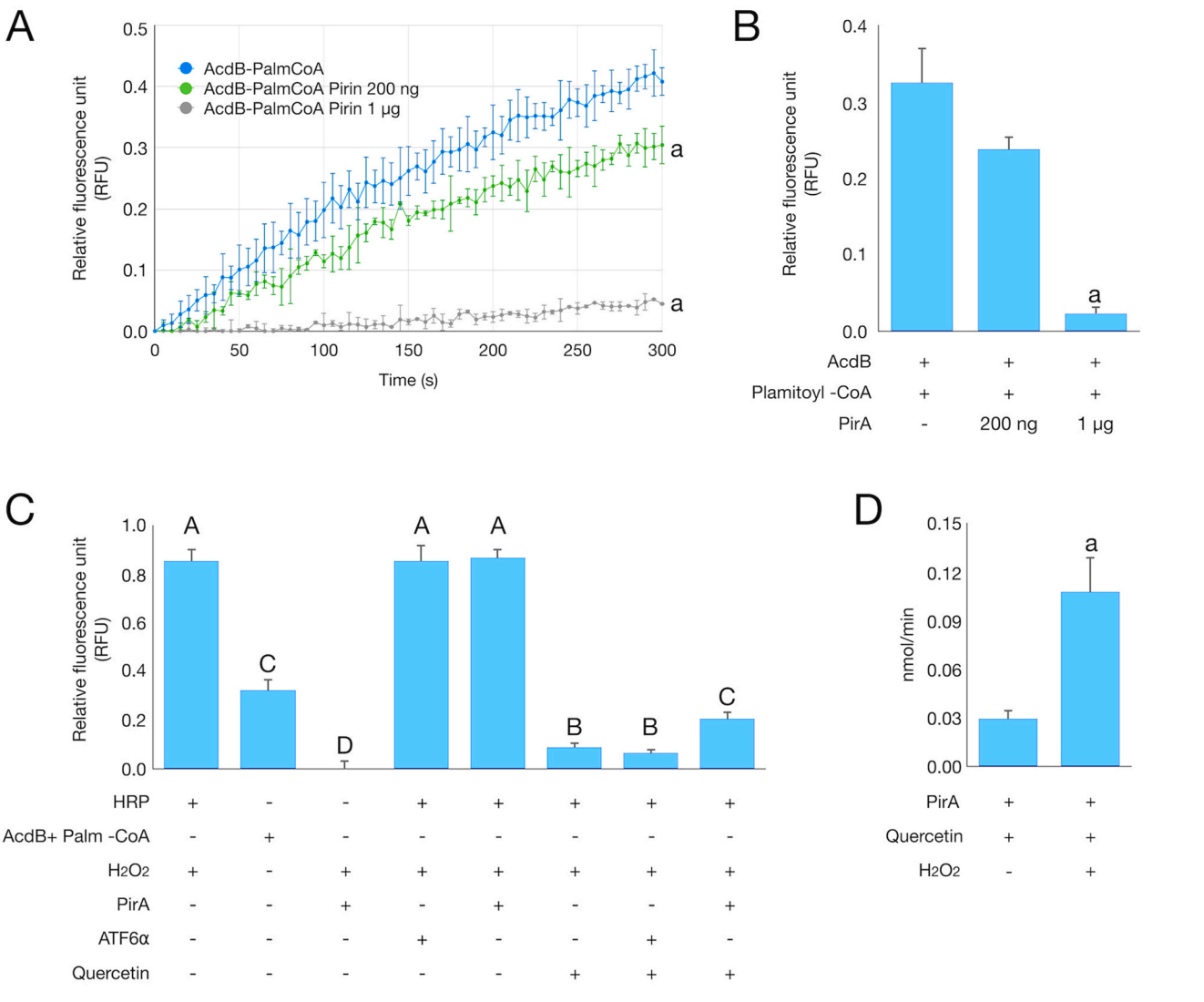

(caption on next page)

Fig. 4. Production of H_2O_2 by *S. ambofaciens* AcdB and quercetinase activity of PirA. A) H_2O_2 production was revealed by dichlorofluorescein (DCF) assay as described in the Materials and Methods section. AcdB was incubated with palmitoyl-CoA in the absence or in the presence of 200 ng - 1 μg PirA, and the fluorescence by oxidized DCF was determined using a fluorometer. The fluorescence values, plotted as relative as fluorescence units (RFU), represented the mean of three independent experiments. B) The histogram represents RFU values recorded at 200 sec. C) Fluorescence from DCF oxidized by H_2O_2 added in the reaction or generated by AcdB/palmitoyl-CoA was reported in histograms. Addition of PirA, but not the control hATF6α attenuated the quercetin quenching of radicals produced by HRP/H_2O_2. Multiple sample comparisons were performed using ANOVA, and uppercase letters (A-D) indicate groups that are not significantly different from each other. D) Quercetinase activity of PirA was determined as described in the Materials and Methods section. In the histogram, quercetinase activity is reported as nmol/min of oxidized quercetin. E) 3D molecular structures and metal binding site of QueD from *Streptomyces* sp. FLA (PDB ID: 5FLI), YhhW from *E. coli* (PDB ID: 6UTS), hPirin (PDB ID: 4EWA), and I-Tasser model of PirA from *S. ambofaciens*. Statistical significances for pairwise comparisons in panels A, B, and D were indicated using the letter a to denote p-values < 0.05 compared to the control samples.

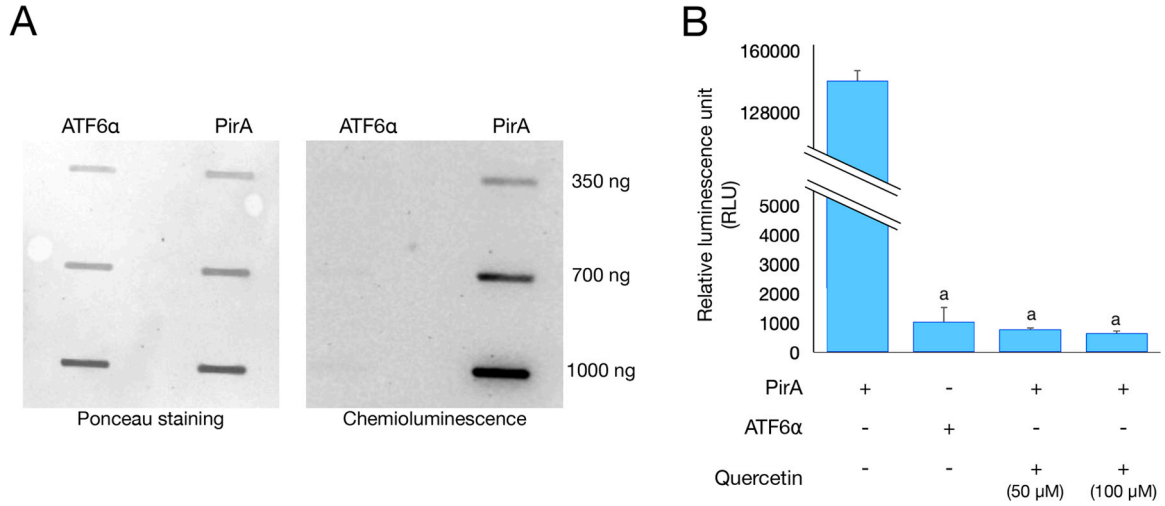

Fig. 5. Luminescence production by PirA in standard enhanced chemiluminescence (ECL) reaction with luminol. A) Purified recombinant PirA and control hATF6α were blotted onto nitrocellulose membrane as indicated in the figure. The red ponceau staining of membrane was reported in the left panel, while the chemiluminescence detected by Chemidoc Image System was reported in the right panel. B) Chemiluminescence generated by PirA in the absence or in the presence of quercetin was quantified by a luminometer. Values recorded as relative luminescence unit (RLU) were reported in histograms. The experiment conducted with hATF6α represented the negative control. The letter a indicates the statistical significance (p-value <0.05) calculated against the assay performed with PirA without quercetin or hATF6α.

FQ762_RS01855 [*catA*]; FQ762_RS39155 [*katA2*]), a gene for a hydroperoxidase II (*katE/catB*) (FQ762_RS03300), and a gene for a catalase/peroxidase HPI (*katG*) (FQ762_RS02765). The phylogenetic relationship between the homologous proteins from *S. ambofaciens* and *Streptomyces coelicolor* A3(2) is shown (Fig. 6A).

In the genomic map of *S. ambofaciens* ATCC 23877 some of these genes are adjacent to genes coding for transcriptional regulator belonging to the ferric uptake regulator (FUR) superfamily (Fig. 6B). Specifically, the gene coding for the catalase SAM23877_RS23675 (down-regulated in *pirA*-defective strain) was adjacent to SAM23877_RS23670 encoding a FUR superfamily regulator highly homologous (identities 97 %, positives 100 %) to *Streptomyces coelicolor* A3(2) CatR (FQ762_RS26925). Furthermore, the gene encoding the catalase/peroxidase HPI (SAM23877_RS33045 [*katG*]) was adjacent to SAM23877_RS33040 coding for another FUR superfamily regulator highly homologous (identities 85 %, positives 90 %) to *Streptomyces coelicolor* A3(2) FurA (FQ762_RS02770).

CatR is of particular interest because in *Streptomyces coelicolor* A3(2) it acts as a negative regulator of the expression of *catA* (FQ762_RS01855), the gene encoding the major vegetative catalase A in response to redox changes (Hahn et al., 2000). Furthermore, it represses transcription of its own *catR* gene allowing rapid adaptation of the system after removal of H_2O_2 by the catalase A (Hahn et al., 2000).

The CatR regulon in *S. coelicolor* A3(2) also include *vtlA*, encoding an exporter protein belonging to the VIT1/CCC1 family protein involved in iron homeostasis through iron extrusion to reduce oxidative stress, and a gene (SCO4983) encoding an unknown protein (Kim et al., 2021). These two genes are conserved in *S. ambofaciens* (Table 1), and expression of *vtlA* (SAM23877_RS09915) has been shown to be transcriptionally down-regulated in *pirA*-defective mutant (Talà et al., 2018).

An accurate analysis of the *catR-catA* intercistronic region revealed the presence of transcriptional promoter elements for divergent *catR* and *catA* transcription predicted by Neural Network Promoter Prediction server (https://www.fruitfly.org/seq_tools/promoter.html) with high score (0.96 for p^{catA} and 0.93 for p^{catR}), and the presence of a canonical CatR motif (TTAGACACTGTCCAT; Table 1) (Kim et al., 2021) overlapping the −10 and −35 promoter regions (Fig. 6C).

An extended analysis of the CatR motif in the genome of *S. ambofaciens* shows that this motif is also present upstream of *vtlA* and the SCO4983 homolog of *S. ambofaciens* (SAM SAM23877_ RS22755), as well as 54 other genes involved in various functions including iron homeostasis and spiramycin biosynthesis (Table S1 of Supplementary Material).

3.9. *Streptomyces PirA interacts with CatR*

The reduced levels of the major vegetative catalase CatA, as well as and *catA* and *catR* mRNA in the *pirA*-deficient strain (Talà et al., 2018) led us to hypothesize a role of PirA in maintaining a basal level of de-repression of the CatR regulon, and a possible involvement of the hydroxyl radicals generated by PirA in this mechanism. This hypothesis is consistent with the postulated regulatory mechanism of CatR, a homologous of PerR of *Bacillus subtilis*, which senses H_2O_2 by metal-catalyzed histidine oxidation promoted by hydroxyl radicals generated by Fenton-type reaction (Lee and Helmann, 2006), as discussed below. Furthermore, PerR proteins display conserved amino acid residues essential for regulatory and metal-binding function, which are also present in CatR. Fig. S4 shows a multiple sequence alignment of

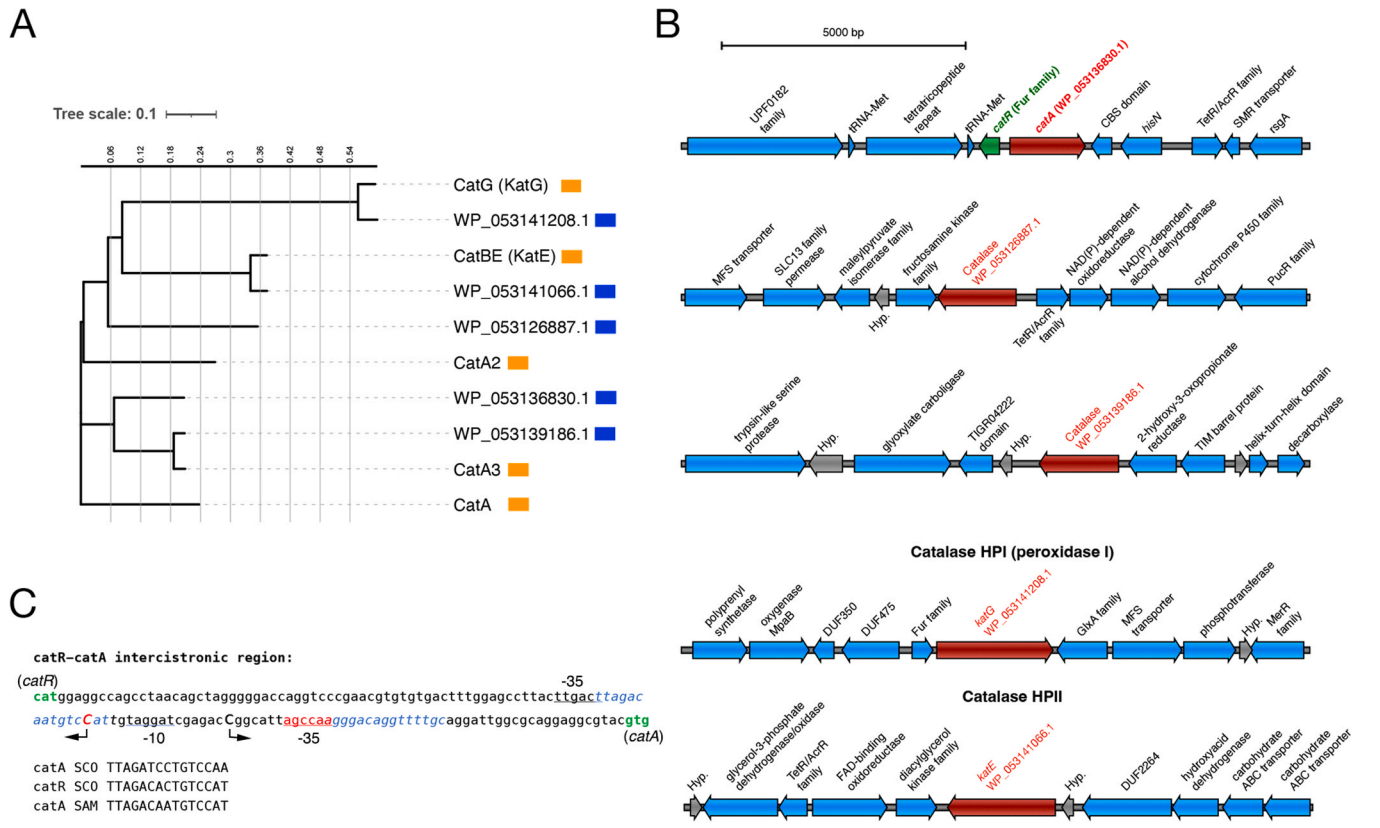

Fig. 6. Genes encoding catalases in *S. ambofaciens*. A) Cladogram comparing the protein sequences of catalases from *S. ambofaciens* (blue squares) and *S. coelicolor* A3 (2) (orange squares). B) Genetic maps of catalase genes in *S. ambofaciens*. Catalase genes are evidenced in red, *catR* (Fur family) gene is evidenced in green. C) Intergenic region between *catR* and *catA* in *S. ambofaciens*. Start codons are shown in green, −35 and −10 promoter elements are underlined. Uppercase letters and arrows indicate the transcription start sites. Elements on the reverse strand are highlighted in red. Putative CatR binding sites are marked in blue. The CatR binding sites in the *catA* and *catR* promoter regions are reported below (SCO = *S. coelicolor* A3[2], SAM = *S. ambofaciens*).

Table 1
CatR-regulated genes in *S. coelicolor* A3(2), homologous genes in *S. ambofaciens*, and alignment of CatR binding motif.

Protein ID SCO	Protein ID SAM	Protein Identity (%)	CatR binding motif	Motif Identity (%)
SCO5206 CatR	WP_053136827.1 CatR	97.10 %	SCO TTAGACACTGTCCAT |||||| |||||| SAM TTAGACAATGTCCAT	93 %
SCO0379 CatA	WP_053136830.1 CatA	57.59 %	SCO TTAGATCCTGTCCAA ||||| ||||| SAM TTAGACAATGTCCAT	66 %
SCO2027 VtlA	WP_053129199.1 VtlA	94.24 %	SCO TTGGACTCGTTCCAC ||||| |||| || SAM TTGGATCAGTTCTAC	73 %
SCO4983 Hypothetical protein	WP_053136333.1 Hypothetical protein	79.29 %	SCO TTAGATCTAATCTAA || ||| |||||| SAM TTGGATTCAATCTAA	80 %

PerR homologs and CatR from *S. ambofaciens* ATCC 23877, highlighting key conserved residues involved in metal binding (regulatory metal sites and zinc-binding Cys-XX-Cys motifs) and residues implicated in metal ion selectivity, which supports the functional conservation of PerR and CatR regulators (Jacquamet et al., 2009; Kim et al., 2011; Lee et al., 2006; Ma et al., 2011; Traore et al., 2006).

Based on these premises, we hypothesized that PirA could physically interact with CatR, regulating its activity through the formation of hydroxyl radicals. The interaction between PirA and CatR was then analyzed *in vitro* by co-purification experiment. His-tagged PirA was incubated with either a control bacterial lysate or a lysate containing overexpressed CatR-V5, followed by recovery using Ni^{2+}-charged resin. The results demonstrated that CatR was co-recovered with PirA, and the specificity of their interaction was confirmed by the absence of a CatR signal in the control experiment (Fig. 7A). Additionally, a control experiment using His-tagged hATF6α protein in the co-elution assay confirmed that the interaction between CatR and PirA was specific (Fig. S5). Moreover, His-tagged PirA and control ATF6 proteins were bound to a nitrocellulose filter in duplicate to perform a slot blot experiment. The two filters were equilibrated with Fe^{2+} or Fe^{3+} cyanate salts, and then incubated in the presence of a bacterial lysate containing overexpressed V5-tagged CatR. At the end of the incubation, the amount of V5-tagged CatR bound to His-tagged PirA or control ATF6 was detected with an anti-V5 antibody for ECL detection (Fig. 7B). Results showed a background ECL signal of PirA in the absence of V5-labeled CatR, due to the ability of PirA to produce luminescence by itself in

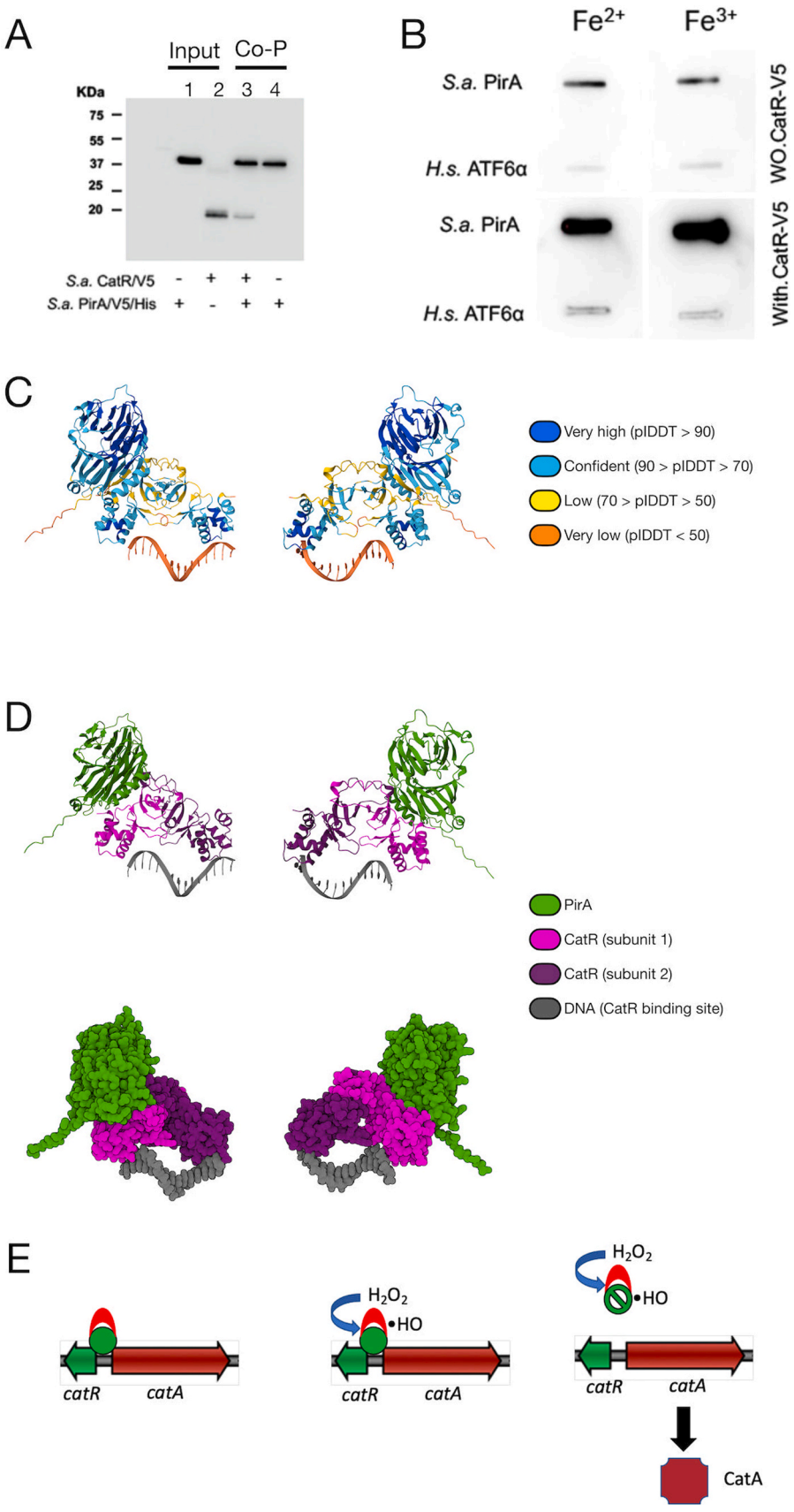

(caption on next page)

Fig. 7. *In vitro* and *in silico* interactions between PirA and CatR. A) Physical interaction between tagged CatR (CatR-V5) and PirA (PirA-V5-His6) was assayed by co-elution experiments using affinity chromatography as detailed in the experimental section. Crude extract lysates from *E. coli* BL21(DE3) transformed with either pET-PirA-V5/His6 (lane 1) or pET-CatR-V5 (lane 2) were used. V5-tagged proteins were detected by Western blotting using antibody against V5 epitope. In lane 3, the two extracts were mixed and challenged by affinity chromatography to detect CatR-V5:PirA-V5/His6 complex formation. In lane 4, extracts from *E. coli* BL21(DE3) transformed with pET-PirA-V5/His6 was challenged with a control extract from *E. coli* BL21(DE3) transformed with pET-21b vector. B) PirA and hATF6α was loaded on nitrocellulose membrane and incubated in a conditioning buffer containing Fe^{2+} (left panels) or Fe^{3+} salts (right panels). Then, membranes were incubated with crude extracts lysates from *E. coli* BL21(DE3) transformed with either pET-PirA-V5/His6 (low panels) or empty pET21b vectors. V5-tagged proteins were detected by ECL using antibody against V5 epitope using a Chemidoc Image system. The histogram on the left shows the densitometric analysis of the slot blot. C and D) Interaction between PirA, CatR and DNA as predicted *in silico*. Model predicted by AlphaFold3 are shown, colored according to prediction quality (C) or partners (D): PirA = green; CatR: light magenta (subunit 1) and dark purple (subunit 2), DNA = gray. E) Functional model of the interaction between PirA and CatR bound at the *catR-catA* operator in the intercistronic region.

the ECL reaction (Fig. 5AB). The ECL signal increased substantially in the presence of V5-tagged CatR, confirming that PirA is able to bind to CatR. The slot blot results also showed that the interaction between PirA and CatR was slightly stronger in the presence of Fe^{3+} than in the presence of Fe^{2+} cyanate salts.

The interaction between PirA and CatR was modeled using the AlphaFold 3 server (Abramson et al., 2024). Based on crystallographic models of Fur family transcriptional regulators from both Gram-positive (Lucarelli et al., 2007) and Gram-negative bacteria (Sarvan et al., 2018), including PerR from *Bacillus subtilis* (Traoré et al., 2006), it was expected that CatR from *S. ambofaciens* forms a dimer. AlphaFold 3 prediction of the complex yielded a model with reasonable overall structure confidence (pTM = 0.55) but low interface confidence (ipTM = 0.25). In particular, the protein complex consisting of the CatR dimer and PirA was predicted with good confidence, whereas the DNA fragment was modeled with lower quality (Fig. 7C). In this model, the two CatR subunits formed a dimer, with both monomers interacting with the DNA, while PirA bound to the dimer on the side opposite the DNA (Fig. 7D).

4. Discussion

This study started from the phylogenetic evidence that associated the occurrence of Pirin family proteins in different prokaryotic and non-prokaryotic taxa with aerobic energy metabolism (Figs. 1 and 2; Fig. S2 and Fig. S3). Pirin family proteins are present in most prokaryotic and non-prokaryotic taxa with aerobic or facultative aerobic/anaerobic metabolism, and absent in anaerobic microorganisms, with some notable exceptions. Indeed, hPirin/PirA orthologs are absent in anaerobic protozoan parasites such as *Giardia* (phylum Metamonada), *Entamoeba* (phylum Sarcomastigophora/Amoebozoa) and *Cryptosporidium* (phylum Apicomplexa), which do not have mitochondria, but mitochondrion-related organelles (MROs) called mitosomes (Santos and Nozaki, 2022). It may be also noted that hPirin/PirA orthologs are absent in aerobic trypanosomatids (Euglenozoa) of the genera *Trypanosoma* and *Leishmania*, which, however, are characterized by compartmentation of enzymes involved in energy metabolism (glycolysis, pentose-phosphate pathway, beta-oxidation of fatty acids, purine salvage, and biosynthetic pathways for pyrimidines, ether-lipids and squalene) into dedicated organelles (Hellemond et al., 2005). All animals belonging to the phylum of Chordata harbors hPirin/PirA orthologs except those belonging to the class of Aves. This unexpected finding may be explained by the fact that Aves have undergone metabolic and physiological adaptations during the evolution of flight. These adaptations are particularly relevant in migratory birds that derive energy from the β-oxidation of fatty acids and have developed biochemical mechanisms to limit β-oxidation-related oxidative stress (Butler, 2016). In fungi, it may be noted the absence of genes encoding Pirin-like proteins in Crabtree-positive yeasts, which are strongly inclined to perform alcoholic fermentation. Indeed, even under fully aerobic conditions, ethanol is produced by these yeasts when sugars are present in excess (van Dijken et al., 1993).

The co-occurrence of *pirA*, *acdB* and *sseB* in the genetic map of streptomycetes and the absence of *pirA* in anaerobic actinomycetaceae (Fig. 2) is consistent with the proposed role of PirA as a redox-sensitive negative modulator of AcdB (vLCAD), which catalyzes the first committed step of the beta-oxidation pathway (Talà et al., 2018). Thus, the next step, in the current study, was to investigate the oxidative stress in *S. ambofaciens pirA*-defective mutant and complemented strain, and, indeed, we found that genetic inactivation of *pirA* resulted in increased intracellular H_2O_2 levels during late exponential and early stationary phases (Fig. 3). We also noted that this increase was more pronounced when the *pirA*-defective mutant was grown in the presence of fatty acids as a carbon source, which led to the hypothesis that AcdB (vLCAD) activity might be an important source of intracellular H_2O_2, as confirmed by *in vitro* experiments (Fig. 4). Thus, in the absence of PirA, intracellular H_2O_2 concentration increases, leading to oxidative stress. However, increased H_2O_2 levels were expected to activate antioxidant systems, and instead proteomic analysis demonstrated down-regulation of catalase CatA, alkylhydroperoxidase, and superoxide dismutase SodF in the *pirA*-deficient strain compared to the wild-type strain (Talà et al., 2018). This result led us to hypothesize that the absence of PirA may determine an alteration in the regulation of antioxidant systems and that PirA may play an important role in such regulation.

The finding that, in the presence of H_2O_2, PirA produced luminescence in the standard enhanced chemiluminescence (ECL) reaction with luminol (Fig. 5) helped us to understand something about the possible role of PirA in the regulation of antioxidant systems of *S. ambofaciens*. Although the chemistry of luminol reaction is very complex, a mechanism was initially proposed by (Roswell and White, 1978). The mechanism involves multiple steps, with a primary oxidation, a secondary oxidation and decomposition of hydroperoxide intermediate, and some of these steps have been studied by (Lind et al., 1983; Merényi et al., 1990) leading to a model. The model proposes formation of luminol diazaquinone hydroperoxide anions ($LOOH^-$) in two steps (primary oxidation and secondary oxidation). Then, $LOOH^-$ spontaneously decompose via a tricyclic endoperoxide transition state to form dinitrogen and excited 3-aminophthalate anions that luminesce. During the primary oxidation step, which usually determines the rate of light emission, hydroxyl radicals (OH•) play a key role. Luminol (LH_2) exists in aqueous solutions at pH 10.0 as monoanions (LH^-). Hydroxyl radicals (OH•) reacting with luminol convert the monoanions (LH^-) to diazasemiquinone radicals ($L^{\bullet-}$ or $LH^{\bullet}$ depending on the pH). During the secondary oxidation, superoxide anions ($O_2^{\bullet-}$), which can also be generated by reaction of H_2O_2 with hydroxyl radicals (OH•) when significant H_2O_2 concentrations are present (Kitajima et al., 1978; McMurray and Wilson, 1999; Ono et al., 1977), react with $L^{\bullet-}$ or $LH^{\bullet}$ to form luminol diazaquinone hydroperoxide anions ($LOOH^-$). Thus, the finding that PirA produced luminescence in the ECL reaction suggested that PirA may form hydroxyl radicals (OH•) in the presence of H_2O_2, through a Fenton-type reaction (Andersen and Harvath, 1979). This reaction may be triggered by release of Fe^{+2} from *Streptomyces* PirA. Indeed, Fe^{+2} bound to proteins is Fenton inactive but can be released from proteins upon attack by activated oxygen (Aust and Koppenol, 1991; Halliwell and Gutteridge, 1986).

We hypothesized that the formation of hydroxyl radicals (OH•) by PirA might be involved in the sensing of peroxides and the activation of antioxidant systems of streptomycetes (Fig. 6). Indeed, in *Streptomyces* CatR acts as a negative regulator of the expression of *catA* and its own

catR gene (Beites et al., 2015; Hahn et al., 2000; Liu et al., 2016). Furthermore, in *Streptomyces avermitilis*, it has been shown that de-repression of the vegetative major catalase gene (*katA1*) occurs through detachment of the CatR repressor from the *katA1-catR* intercistronic promoter region and subsequent binding of the OxyR activator (Liu et al., 2016). CatR is highly homologous to PerR that in *Bacillus subtilis* regulates the expression of antioxidant systems by a mechanism involving hydroxyl radicals (OH•). PerR represses the expression of its own *perR* gene, as well as other genes involved in oxidative stress response (*katA*, *ahpCF*, *mrgA*) and metal homeostasis (*zosA*, *fur*, *hemA* operon) (Dubbs and Mongkolsuk, 2012). At variance with other bacterial proteins including OxyR, OhrR abd Hsp33, which senses peroxides by redox-active cysteines, PerR senses H_2O_2 by metal-catalyzed histidine oxidation (Lee and Helmann, 2006). In particular, PerR has two metal-binding sites: a structural Zn^{2+}-binding site, and a regulatory Fe^{+2} (or Mn^{+2}) binding site. Upon peroxide exposure, the hydroxyl radicals generated by Fenton-type reaction of bound Fe^{+2} rapidly react with the histidine residues that coordinate the bound Fe^{+2} leading to the formation of 2-oxo-histidine residues and inactivation of PerR, which results in de-repression of the genes of the PerR regulon (Lee and Helmann, 2006). Therefore, the generation of hydroxyl radicals is critical for CatR inactivation and de-repression of the CatR regulon.

Thus, we hypothesized that PirA could physically interact with CatR and, indeed, we found that PirA was able to interact with CatR *in vitro* (Fig. 7AB). The interaction between PirA, CatR and DNA may occur as predicted *in silico* (Fig. 7CD). Although this represents the first evidence of the direct involvement of Pirin-like proteins in the control of antioxidant systems of Gram-positive bacteria, future experiments are needed to understand whether hydroxyl radical production by PirA is actually necessary or contributes to the inactivation of CatR and hence to its dissociation from the *catA* promoter with consequent de-repression of *catA*, as proposed in our model (Fig. 7E).

CRediT authorship contribution statement

Adelfia Talà: Writing – review & editing. **Fabrizio Damiano:** Writing – review & editing, Investigation, Formal analysis. **Pietro Alifano:** Writing – review & editing, Writing – original draft, Supervision, Project administration, Formal analysis. **Matteo Calcagnile:** Writing – review & editing, Investigation, Formal analysis.

Funding

The research reported in this study was partially funded by the European Union - Next Generation EU, Mission 4 Component 1 CUP J53D23010040006 to AT (grant assignment decree n. 1326 adopted on 10/08/2023 by Italian Ministry of University and Research, project code 2022J7W7LW), and by university funds (Basic Research Fund, D.R. 936/2024) to PA, AT and FD.

Appendix A. Supporting information

Supplementary data associated with this article can be found in the online version at doi:10.1016/j.micres.2025.128310.

Data availability

No data was used for the research described in the article.

References

Abramson, J., Adler, J., Dunger, J., Evans, R., Green, T., Pritzel, A., Ronneberger, O., Willmore, L., Ballard, A.J., Bambrick, J., Bodenstein, S.W., Evans, D.A., Hung, C.C., O'Neill, M., Reiman, D., Tunyasuvunakool, K., Wu, Z., Žemgulytė, A., Arvaniti, E., Beattie, C., Bertolli, O., Bridgland, A., Cherepanov, A., Congreve, M., Cowen-Rivers, A.I., Cowie, A., Figurnov, M., Fuchs, F.B., Gladman, H., Jain, R., Khan, Y.A., Low, C.M.R., Perlin, K., Potapenko, A., Savy, P., Singh, S., Stecula, A., Thillaisundaram, A., Tong, C., Yakneen, S., Zhong, E.D., Zielinski, M., Žídek, A., Bapst, V., Kohli, P., Jaderberg, M., Hassabis, D., Jumper, J.M., 2024. Accurate structure prediction of biomolecular interactions with AlphaFold 3. Nature 630 (8016), 493–500. https://doi.org/10.1038/s41586-024-07487-w.

Adams, M., Jia, Z., 2005. Structural and biochemical analysis reveal pirins to possess quercetinase activity, 282 J. Biol. Chem. 280 (31), 28675. https://doi.org/10.1074/jbc.M501034200.

Andersen, B.R., Harvath, L., 1979. Light generation with fenton's reagent. Its relationship to granulocyte chemiluminescence. Biochim Biophys. Acta 584 (1), 164–173. https://doi.org/10.1016/0304-4165(79)90246-0.

Aust, S.D., Koppenol, W.H., 1991. Transition metals in oxidative stress: an overview. In: Davies, K.J.A. (Ed.), Oxidative Damage and Repair. Pergamon Press, Oxford, pp. 802–807.

Bailey, T.L., Johnson, J., Grant, C.E., Noble, W.S., 2015. The MEME suite. Nucleic Acids Res. 43 (W1), W39–W49.

Beites, T., Oliveira, P., Rioseras, B., Pires, S.D., Oliveira, R., Tamagnini, P., Moradas-Ferreira, P., Manteca, Á., Mendes, M.V., 2015 Aug 10. *streptomyces natalensis* programmed cell death and morphological differentiation are dependent on oxidative stress. Sci. Rep. 5, 12887. https://doi.org/10.1038/srep12887.

Berman, H.M., Westbrook, J., Feng, Z., Gilliland, G., Bhat, T.N., Weissig, H., Shindyalov, I.N., Bourne, P.E., 2000. The protein data bank. Nucleic Acids Res. 28 (1), 235–242. https://doi.org/10.1093/nar/28.1.235.

Bowater, L., Fairhurst, S.A., Just, V.J., Bornemann, S., 2004. *bacillus subtilis* YxaG is a novel Fe-containing quercetin 2,3-dioxygenase. FEBS Lett. 557 (1–3), 45–48. https://doi.org/10.1016/s0014-5793(03)01439-x.

Buonvino, S., Arciero, I., Melino, S., 2022. Thiosulfate-Cyanide sulfurtransferase a mitochondrial essential enzyme: from cell metabolism to the biotechnological applications. Int J. Mol. Sci. 23 (15), 8452. https://doi.org/10.3390/ijms23158452.

Butler, P.J., 2016. The physiological basis of bird flight. Philos. Trans. R. Soc. Lond. B Biol. Sci. 371 (1704), 20150384. https://doi.org/10.1098/rstb.2015.0384.

Calcagnile, M., Bettini, S., Damiano, F., Talà, A., Tredici, S.M., Pagano, R., Di Salvo, M., Siculella, L., Fico, D., De Benedetto, G.E., Valli, L., Alifano, P., 2018. Stimulatory effects of Methyl-β-cyclodextrin on spiramycin production and Physical-Chemical characterization of Nonhost@Guest complexes. ACS Omega 3 (3), 2470–2478. https://doi.org/10.1021/acsomega.7b01766.

Cipollone, R., Ascenzi, P., Visca, P., 2007. Common themes and variations in the rhodanese superfamily. IUBMB Life 59 (2), 51–59. https://doi.org/10.1080/15216540701206859.

Dechend, R., Hirano, F., Lehmann, K., Heissmeyer, V., Ansieau, S., Wulczyn, F.G., Scheidereit, C., Leutz, A., 1999. The Bcl-3 oncoprotein acts as a bridging factor between NF-kappaB/Rel and nuclear co-regulators. Oncogene 18 (22), 3316–3323. https://doi.org/10.1038/sj.onc.1202717.

van Dijken, J.P., Weusthuis, R.A., Pronk, J.T., 1993. Kinetics of growth and sugar consumption in yeasts. Antonie Van. Leeuwenhoek 63 (3–4), 343–352. https://doi.org/10.1007/BF00871229.

Doi, H., Hoshino, Y., Nakase, K., Usuda, Y., 2014. Reduction of hydrogen peroxide stress derived from fatty acid beta-oxidation improves fatty acid utilization in escherichia coli. Appl. Microbiol Biotechnol. 98 (2), 629–639. https://doi.org/10.1007/s00253-013-5327-6.

Dubbs, J.M., Mongkolsuk, S., 2012. Peroxide-sensing transcriptional regulators in bacteria. J. Bacteriol. 194 (20), 5495–5503. https://doi.org/10.1128/JB.00304-12.

Gomez, C.A.D., Neubig, R., Lisabeth, E.M., 2023. Revisiting pirin: evidence for a role in translational but not in transcriptional control. J. Pharm. Exp. Ther. 385 (S3), 526. https://doi.org/10.1124/jpet.122.551800.

Grant, C.E., Bailey, T.L., Noble, W.S., 2011. FIMO: scanning for occurrences of a given motif. Bioinformatics 27 (7), 1017–1018.

Guo, B., Zhang, Y., Hicks, G., Huang, X., Li, R., Roy, N., Jia, Z., 2019. Structure-Dependent modulation of substrate binding and biodegradation activity of pirin proteins toward plant flavonols. ACS Chem. Biol. 14 (12), 2629–2640. https://doi.org/10.1021/acschembio.9b00575.

Gurmu, D., Lu, J., Johnson, K.A., Nordlund, P., Holmgren, A., Erlandsen, H., 2009. The crystal structure of the protein YhaK from escherichia coli reveals a new subclass of redox sensitive enterobacterial bicupins. Proteins 74 (1), 18–31. https://doi.org/10.1002/prot.22128.

Hahn, J.S., Oh, S.Y., Chater, K.F., Cho, Y.H., Roe, J.H., 2000. H_2O_2-sensitive fur-like repressor CatR regulating the major catalase gene in streptomyces coelicolor. J. Biol. Chem. 275 (49), 38254–38260. https://doi.org/10.1074/jbc.M006079200.

Halliwell, B., Gutteridge, J.M.C., 1986. Iron and free radical reactions: two aspects of antioxidant protection. Trends Biochem. Sci. 11, 372–375.

Hellemond, J.J., Bakker, B.M., Tielens, A.G., 2005. Energy metabolism and its compartmentation in trypanosoma brucei. Adv. Microb. Physiol. 50, 199–226. https://doi.org/10.1016/S0065-2911(05)50005-5.

Hihara, Y., Muramatsu, M., Nakamura, K., Sonoike, K., 2004. A cyanobacterial gene encoding an ortholog of pirin is induced under stress conditions. FEBS Lett. 574 (1-3), 101–105. https://doi.org/10.1016/j.febslet.2004.06.102.

Jacquamet, L., Traoré, D.A., Ferrer, J.L., Proux, O., Testemale, D., Hazemann, J.L., Nazarenko, E., El Ghazouani, A., Caux-Thang, C., Duarte, V., Latour, J.M., 2009 Jul. Structural characterization of the active form of PerR: insights into the metal-induced activation of PerR and fur proteins for DNA binding. Mol. Microbiol. 73 (1), 20–31. https://doi.org/10.1111/j.1365-2958.2009.06753.x.

Jeoung, J.H., Nianios, D., Fetzner, S., Dobbek, H., 2016. Quercetin 2,4-Dioxygenase activates dioxygen in a Side-On O_2-Ni complex. Angew. Chem. Int. Ed. 55 (10), 3281–3284. https://doi.org/10.1002/anie.201510741.

Kakimoto, P.A., Tamaki, F.K., Cardoso, A.R., Marana, S.R., Kowaltowski, A.J., 2015. H_2O_2 release from the very long chain acyl-CoA dehydrogenase. Redox Biol. 4, 375–380. https://doi.org/10.1016/j.redox.2015.02.003.

Kim, M., Hwang, S., Ryu, S., Jeon, B., 2011. Regulation of perr expression by iron and PerR in campylobacter jejuni. J. Bacteriol. 193 (22), 6171–6178.
Kim, Y., Roe, J.H., Park, J.H., Cho, Y.J., Lee, K.L., 2021. Regulation of iron homeostasis by peroxide-sensitive CatR, a Fur-family regulator in streptomyces coelicolor. J. Microbiol. 59 (12), 1083–1091. https://doi.org/10.1007/s12275-021-1457-1.
Kim, Y.M., Lim, J.M., Kim, B.C., Han, S., 2006. Cu,Zn-superoxide dismutase is an intracellular catalyst for the H_2O_2-dependent oxidation of dichlorodihydrofluorescein. Mol. Cells 21 (1), 161–165.
Kitajima, N., Fukuzumi, S.-I., Ono, Y., 1978. Formation of superoxide ion during the decomposition of hydrogen peroxide on supported metal oxides. J. Phys. Chem. 82 (13), 1505–1509. https://doi.org/10.1021/j100502a009.
Kruithof, P.D., Lunev, S., Aguilar Lozano, S.P., de Assis Batista, F., Al-Dahmani, Z.M., Joles, J.A., Dolga, A.M., Groves, M.R., van Goor, H., 2020. Unraveling the role of thiosulfate sulfurtransferase in metabolic diseases. Biochim. Et. Biophys. Acta Mol. Basis Dis. 1866 (6), 165716. https://doi.org/10.1016/j.bbadis.2020.165716.
Lapik, Y.R., Kaufman, L.S., 2003. The arabidopsis cupin domain protein AtPirin1 interacts with the g protein alpha-subunit GPA1 and regulates seed germination and early seedling development. Plant Cell 15 (7), 1578–1590. https://doi.org/10.1105/tpc.011890.
Lauchnor, E.G., Radniecki, T.S., Semprini, L., 2011. Inhibition and gene expression of *nitrosomonas europaea* biofilms exposed to phenol and toluene. Biotechnol. Bioeng. 108 (4), 750–757. https://doi.org/10.1002/bit.22999.
LeBel, C.P., Ischiropoulos, H., Bondy, S.C., 1992. Evaluation of the probe 2′,7′-dichlorofluorescin as an indicator of reactive oxygen species formation and oxidative stress. Chem. Res. Toxicol. 5 (2), 227–231. https://doi.org/10.1021/tx00026a012.
Lee, J.W., Helmann, J.D., 2006. The PerR transcription factor senses H2O2 by metal-catalysed histidine oxidation. Nature 440 (7082), 363–367. https://doi.org/10.1038/nature04537.
Letunic, I., Bork, P., 2021. Interactive tree of life (iTOL) v5: an online tool for phylogenetic tree display and annotation. Nucleic Acids Res. 49 (W1), W293–W296. https://doi.org/10.1093/nar/gkab301.
Lind, J., Merenyi, G., Eriksen, T.E., 1983. Chemiluminescence mechanism of cyclic hydrazides such as luminol in aqueous solutions. J. Am. Chem. Soc. 105 (26), 7655–7661. https://doi.org/10.1021/ja00364a032.
Liu, F., Rehmani, I., Esaki, S., Fu, R., Chen, L., de Serrano, V., Liu, A., 2013. Pirin is an iron-dependent redox regulator of NF-κB. Proc. Natl. Acad. Sci. USA 110 (24), 9722–9727. https://doi.org/10.1073/pnas.1221743110.
Liu, X., Sun, M., Cheng, Y., Yang, R., Wen, Y., Chen, Z., Li, J., 2016 Apr. OxyR is a key regulator in response to oxidative stress in *streptomyces avermitilis*. Microbiology 162 (4), 707–716. https://doi.org/10.1099/mic.0.000251.
Lounès, A., Lebrihi, A., Benslimane, C., Lefebvre, G., Germain, P., 1996. Regulation of spiramycin synthesis in *streptomyces ambofaciens*: effects of glucose and inorganic phosphate. Appl. Microbiol. Biotechnol. 45 (1-2), 204–211. https://doi.org/10.1007/s002530050671.
Lucarelli, D., Russo, S., Garman, E., Milano, A., Meyer-Klaucke, W., Pohl, E., 2007. Crystal structure and function of the zinc uptake regulator FurB from *mycobacterium tuberculosis*. J. Biol. Chem. 282 (13), 9914–9922. https://doi.org/10.1074/jbc.M609974200.
Ma, Z., Lee, J.W., Helmann, J.D., 2011. Identification of altered function alleles that affect bacillus subtilis PerR metal ion selectivity. Nucleic Acids Res. 39, 5036–5044.
Mancini, A., Imperlini, E., Nigro, E., Montagnese, C., Daniele, A., Orrù, S., Buono, P., 2015. Biological and nutritional properties of palm oil and palmitic acid: effects on health. Molecules 20 (9), 17339–17361. https://doi.org/10.3390/molecules200917339.
McMurray, H.N., Wilson, B.P., 1999. Mechanistic and spatial study of ultrasonically induced luminol chemiluminescence. J. Phys. Chem. A 103, 3955–3962. https://doi.org/10.1021/jp984503r.
Merényi, G., Lind, J., Eriksen, T.E., 1990. Luminol chemiluminescence: chemistry, excitation, emitter. J. Biolumin. Chemilumin. 5 (1), 53–56. https://doi.org/10.1002/bio.1170050111.
Merkens, H., Sielker, S., Rose, K., Fetzner, S., 2007. A new monocupin quercetinase of *streptomyces* sp. Fla: identification and heterologous expression of the qued gene and activity of the recombinant enzyme towards different flavonols. Arch. Microbiol. 187 (6), 475–487. https://doi.org/10.1007/s00203-007-0215-z.
Meschkewitz, M., Lisabeth, E.M., Neubig, R., 2023. Without a trace: the pirin and NF-kB interaction. J. Pharmacol. Exp. Ther. 385 (S3), 82. https://doi.org/10.1124/jpet.122.264930.
Oberg, N., Zallot, R., Gerlt, J.A., 2023. EFI-EST, EFI-GNT, and EFI-CGFP: enzyme function initiative (EFI) web resource for genomic enzymology tools. J. Mol. Biol. 435 (14), 168018. https://doi.org/10.1016/j.jmb.2023.168018.
Ono, Y., Matsumura, T., Kitajima, N., Fukuzumi, S.-I., 1977. Formation of superoxide ion during the decomposition of hydrogen peroxide on supported metals. J. Phys. Chem. 81 (13), 1307–1311. https://doi.org/10.1021/j100528a018.
Orzaez, D., de Jong, A.J., Woltering, E.J., 2001. A tomato homologue of the human protein PIRIN is induced during programmed cell death. Plant Mol. Biol. 46 (4), 459–468. https://doi.org/10.1023/a:1010618515051.
Papuc, C., Goran, G.V., Predescu, C.N., Nicorescu, V., Stefan, G., 2017. Plant polyphenols as antioxidant and antibacterial agents for shelf-life extension of meat and meat products: classification, structures, sources, and action mechanisms. Compr. Rev. Food Sci. Food Saf. 16 (6), 1243–1268. https://doi.org/10.1111/1541-4337.12298.
Paysan-Lafosse, T., Blum, M., Chuguransky, S., Grego, T., Pinto, B.L., Salazar, G.A., Bileschi, M.L., Bork, P., Bridge, A., Colwell, L., Gough, J., Haft, D.H., Letunic, I., Marchler-Bauer, A., Mi, H., Natale, D.A., Orengo, C.A., Pandurangan, A.P., Rivoire, C., Sigrist, C.J.A., Sillitoe, I., Thanki, N., Thomas, P.D., Tosatto, S.C.E., Wu, C.H., Bateman, A., 2023. InterPro in 2022. Nucleic Acids Res. 51 (D1), D418–D427. https://doi.org/10.1093/nar/gkac993.
Pettersen, E.F., Goddard, T.D., Huang, C.C., Couch, G.S., Greenblatt, D.M., Meng, E.C., Ferrin, T.E., 2004. UCSF Chimera—a visualization system for exploratory research and analysis. J. Comput. Chem. 25 (13), 1605–1612. https://doi.org/10.1002/jcc.20084.
Quinlan, A.R., 2014. BEDTools: the Swiss-army tool for genome feature analysis. Curr. Protoc. Bioinforma. 47 (1), 11–12.
Roswell, D.F., White, E.W., 1978. The chemiluminescence of luminol and related hydrazides. Methods Enzymol. 57, 409–423. https://doi.org/10.1016/0076-6879(78)57038-9.
Santos, H.J., Nozaki, T., 2022. The mitosome of the anaerobic parasitic protist entamoeba histolytica: a peculiar and minimalist mitochondrion-related organelle. J. Eukaryot. Microbiol. 69 (6), e12923. https://doi.org/10.1111/jeu.12923.
Sarvan, S., Charih, F., Butcher, J., Brunzelle, J.S., Stintzi, A., Couture, J.F., 2018. Crystal structure of campylobacter jejuni peroxide regulator. FEBS Lett. 592 (13), 2351–2360. https://doi.org/10.1002/1873-3468.13120.
Shannon, P., Markiel, A., Ozier, O., Baliga, N.S., Wang, J.T., Ramage, D., Amin, N., Schwikowski, B., Ideker, T., 2003. Cytoscape: a software environment for integrated models of biomolecular interaction networks. Genome Res. 13 (11), 2498–2504. https://doi.org/10.1101/gr.1239303.
Sievers, F., Higgins, D.G., 2021. The clustal omega multiple alignment package. Methods Mol. Biol. 2231, 3–16. https://doi.org/10.1007/978-1-0716-1036-7_1.
Soo, P.C., Horng, Y.T., Lai, M.J., Wei, J.R., Hsieh, S.C., Chang, Y.L., Tsai, Y.H., Lai, H.C., 2007. Pirin regulates pyruvate catabolism by interacting with the pyruvate dehydrogenase E1 subunit and modulating pyruvate dehydrogenase activity. J. Bacteriol. 189 (1), 109–118. https://doi.org/10.1128/JB.00710-06.
Steiner, R.A., Kalk, K.H., Dijkstra, B.W., 2002. Anaerobic enzyme-substrate structures provide insight into the reaction mechanism of the copper-dependent quercetin 2,3-dioxygenase. PNAS 99 (26), 16625–16630. https://doi.org/10.1073/pnas.262506299.
Szklarczyk, D., Kirsch, R., Koutrouli, M., Nastou, K., Mehryary, F., Hachilif, R., Gable, A. L., Fang, T., Doncheva, N.T., Pyysalo, S., Bork, P., Jensen, L.J., von Mering, C., 2023. The STRING database in 2023: protein-protein association networks and functional enrichment analyses for any sequenced genome of interest. Nucleic Acids Res. 51 (D1), D638–D646. https://doi.org/10.1093/nar/gkac1000.
Talà, A., Damiano, F., Gallo, G., Pinatel, E., Calcagnile, M., Testini, M., Fico, D., Rizzo, D., Sutera, A., Renzone, G., Scaloni, A., De Bellis, G., Siculella, L., De Benedetto, G.E., Puglia, A.M., Peano, C., Alifano, P., 2018. Pirin: a novel redox-sensitive modulator of primary and secondary metabolism in streptomyces. Metab. Eng. 48, 254–268. https://doi.org/10.1016/j.ymben.2018.06.008.
Tranchimand, S., Ertel, G., Gaydou, V., Gaudin, C., Tron, T., Iacazio, G., 2008. Biochemical and molecular characterization of a quercetinase from penicillium olsonii. Biochimie 90 (5), 781–789. https://doi.org/10.1016/j.biochi.2007.12.004.
Tranchimand, S., Brouant, P., Iacazio, G., 2010. The rutin catabolic pathway with special emphasis on quercetinase. Biodegradation 21 (6), 833–859. https://doi.org/10.1007/s10532-010-9359-7.
Traoré, D.A., El Ghazouani, A., Ilango, S., Dupuy, J., Jacquamet, L., Ferrer, J.L., Caux-Thang, C., Duarte, V., Latour, J.M., 2006. Crystal structure of the apo-PerR-Zn protein from bacillus subtilis. Mol. Microbiol. 61 (5), 1211–1219. https://doi.org/10.1111/j.1365-2958.2006.05313.x.
Wendler, W.M., Kremmer, E., Förster, R., Winnacker, E.L., 1997. Identification of pirin, a novel highly conserved nuclear protein. J. Biol. Chem. 272 (13), 8482–8489.
Widiatningrum, T., Maeda, S., Kataoka, K., Sakurai, T., 2015. A pirin-like protein from pseudomonas stutzeri and its quercetinase activity. Biochem. Biophys. Rep. 3, 144–149. https://doi.org/10.1016/j.bbrep.2015.08.001.
Yang, J., Zhang, Y., 2015. I-TASSER server: new development for protein structure and function predictions. Nucleic Acids Res. 43 (W1), W174–W181. https://doi.org/10.1093/nar/gkv342.
Zhang, Y., Bharathi, S.S., Beck, M.E., Goetzman, E.S., 2019. The fatty acid oxidation enzyme long-chain acyl-CoA dehydrogenase can be a source of mitochondrial hydrogen peroxide. Redox Biol. 26, 101253. https://doi.org/10.1016/j.redox.2019.101253.